Research Article

Zhigang Yi*, Tao Jiang, Ying Cheng, and Qiong Tang*

Effect of SiO_2 aerogels loading on photocatalytic degradation of nitrobenzene using composites with tetrapod-like ZnO

https://doi.org/10.1515/ntrev-2020-0081
received April 20, 2020; accepted October 01, 2020

Abstract: To study the effect of improved adsorption property of tetrapod-like ZnO (T-ZnO) on its photocatalytic performance, a new composite was prepared by loading silica aerogels (SiO_2(AG)) on the surface of T-ZnO via the sol–gel method. Various characterization methods showed that SiO_2(AG) was uniformly loaded on the surface of T-ZnO, and the morphology as well as structural characteristics of SiO_2(AG) and T-ZnO were not changed. Nitrobenzene (NB) was selected as the model pollutant, and the adsorption and photocatalytic properties of T-ZnO and SiO_2(AG)/T-ZnO for NB were studied. The photocatalytic degradation processes of NB using T-ZnO and SiO_2(AG)/T-ZnO followed the first-order reaction. Considering the initial moment reaction kinetic, the photocatalytic kinetic of SiO_2(AG)/T-ZnO and T-ZnO was consistent with the Langmuir–Hinshelwood kinetic model, and reaction rate constant $k'_{SiO_2(AG)/T\text{-}ZnO} > k'_{T\text{-}ZnO}$, adsorption rate constant $K_{ad\ SiO_2(AG)/T\text{-}ZnO} > K_{ad\ T\text{-}ZnO}$, which demonstrated that SiO_2(AG) loading could increase T-ZnO adsorption to NB, then promoted its photocatalytic performance.

Keywords: silica aerogels, tetrapod-like zinc oxide, adsorption property, photocatalytic performance, nitrobenzene

1 Introduction

In recent years, large varieties of nanomaterials have become research hotspots in the fields of medicine [1–4], architecture [5–7], energy storage [8,9], and environmental protection [10–14] due to their many special properties such as good chemical stability, microwave absorption, high surface activity, and strong oxidation. Nanomaterials have been investigated in-depth for environmental pollutant treatment [15–19] because of the environmental problems caused by the discharge of persistent organic pollutants with rapid development of industry [20–23].

In the past few decades, more and more attention has been paid to nanomaterial photocatalytic technology, which uses natural/UV light as energy and semiconductor nanomaterials as photocatalysts to degrade organic contaminates via the photocatalytic process on the surface of nanomaterials [24–26]. Among the semiconductors employed, although TiO_2 is generally regarded as the best photocatalyst, ZnO has frequently exhibited similar or higher photocatalytic activity compared to TiO_2 [27–32]. In addition, ZnO has the advantages of low cost and easy preparation [33]. All of these make ZnO an ideal substitute for TiO_2. Previous studies of our research group have found that the microsized tetrapod-like zinc oxide (T-ZnO) had better photocatalytic activity and dispersion than nanosized ZnO with other different morphologies, and was easier to separate from water for reusage [20]. Among different factors affecting the efficiency of photocatalytic degradation of organic matter, the adsorption behaviors of the contaminants onto the surface of photocatalyst were typically considered to play significant roles [34–36]. Plenty of studies have shown that adsorption behaviors were necessary for successful photocatalytic decomposition of organic compounds [37,38]. Thus, improving adsorption property of T-ZnO on the basis of keeping its morphology has been a major consideration to further improve the photocatalytic performance of T-ZnO.

* **Corresponding author: Zhigang Yi,** Department of Chemistry, Leshan Normal University, Leshan, 614004, China, e-mail: 531609732@qq.com, tel: +86-83-32-27-0785; fax: +86-83-32-27-0785
* **Corresponding author: Qiong Tang,** Department of Chemistry, Leshan Normal University, Leshan, 614004, China, e-mail: tangqiong75@163.com
Tao Jiang, Ying Cheng: Department of Chemistry, Leshan Normal University, Leshan, 614004, China

In recent years, porous materials such as activated carbon, zeolites, and SiO_2 were actively investigated as advanced sorbents [39]. Many of these porous materials have been used as support materials; loading of TiO_2, ZnO, and other semiconductors in the porous materials has improved their adsorption and photocatalytic activity [40–42]. One of the promising porous materials, SiO_2 aerogels (SiO_2(AG)), is a three-dimensional and multiscaled porous nanomaterial formed by numerous fine particles and networks. The SiO_2(AG) materials possess excellent adsorption efficiency owing to high porosity, high specific surface area (SSA), low density, etc. [39,43,44].

To study the effect of improved adsorption property of T-ZnO on its photocatalytic performance, we prepared SiO_2(AG)/T-ZnO composites via the sol–gel method, and nitrobenzene (NB) was selected as the model pollutant. The absorption and photocatalytic properties of T-ZnO and SiO_2(AG)/T-ZnO for NB were comparatively studied. The Langmuir–Hinshelwood kinetic model was used to calculate the photodegradation kinetic parameter.

2 Experimental

2.1 Reagents and materials

T-ZnO, received from Key Laboratory of Advanced technologies of Materials (Ministry of Education), Southwest Jiaotong University, was prepared by the gas-expanding method using metallic zinc as the raw material [45]. Tetraethyl orthosilicate, anhydrous ethanol (EtOH), trimethylchlorosilane, hexane, HCl, $NH_3{\cdot}H_2O$, and NB were commercially purchased. All reagents were of analytical-grade quality and used without further purification. Deionized water was used in all experiments.

2.2 Preparation of SiO_2(AG)/T-ZnO

The SiO_2(AG) was synthesized by the solvent-exchanging procedure under ambient pressure as described in our earlier report [20]. The SiO_2(AG) powders were dispersed with hexane under ultrasonic assistance to form a fluid sol dispersion [46]. The designated amounts of T-ZnO were mixed into the sol, and after stirring at 60°C for 2 h, the SiO_2 gel was deposited onto the surface of T-ZnO. SiO_2(AG)/T-ZnO composites were obtained after washing with EtOH and drying at 60°C for 24 h.

2.3 Material characterization

The FESEM (Inspect F; FEI, Holland, the Netherlands) and FETEM (JEM-2100F; JEOL, Japan) were used to investigate the microtopography of fabricated materials. The crystal structure of the materials was analyzed by X-ray diffraction (XRD DX-2500) with Cu Kα-ray generator (40 kV, 40 mA, λ = 0.15406 nm). The pore structure and the SSA of the prepared materials were determined by the automatic porosity and surface area analyzer (3H-2000PS4; Beishide Instrument Technology Co., Ltd, Beijing, China), respectively, and the detecting conditions of analyzer were as follows: nitrogen as adsorbate, degassing mode of heating vacuum, degassing temperature of 150°C, degassing time of 180 min, saturated steam pressure of 1.0434 bar, and ambient temperature of 14.0°C. UV-VIS diffuse reflectance spectra (UV-VIS DRS) were measured using a TU-1901 spectrophotometer (Purkinje General).

2.4 Research of adsorption performance

Isothermal adsorption experiments were conducted in NB solution with different concentrations (12, 24, 36, 48, and 60 mg/L). The dosage of adsorbent (T-ZnO and SiO_2(AG)/T-ZnO) was 2.0 g/L. NB solution of different concentrations (100 mL) was placed in a 250 mL conical flask and shaken at 220 rpm for 24 h under 25°C. The adsorption amount of NB on adsorbent was reflected by measuring the change of concentration of NB in solution via the UV-VIS spectrophotometer (UV-2550; Shimadzu, Japan), which was calculated by:

$$q = \frac{(C_0 - C_e) \times v}{w}, \tag{1}$$

where q is the adsorption amount of NB on adsorbent, mg/g; C_0 is the initial concentration of NB in solution, mg/L; C_e is the equilibrium adsorption concentration of NB in solution after adsorption equilibrium, mg/L; v is the volume of solution, L; and w is the dosage of adsorbent, g.

2.5 Photocatalytic performance

NB solution with different concentrations (12, 24, 36, 48, and 60 mg/L) was used as simulated wastewater. The dosage of photocatalyst (T-ZnO and SiO_2(AG)/T-ZnO) was 2 g/L, respectively. The suspension was stirred for 30 min at room temperature under dark condition, then irradiated

under UV (EA-180, 8w; Spectronics Corporation, America). The sample was fetched at an interval of 30 min, then centrifuged (8,000 rpm, 5 min), and filtered (0.22 μm filter membrane). UV-VIS spectrophotometer was used to analyze the concentration change of NB during the photocatalytic degradation process. Formula of photocatalytic removal ratio of NB is as follows:

$$\eta\% = \frac{C_0 - C}{C_0}, \tag{2}$$

where η% is the photocatalytic removal ratio of NB; C_0 is the initial concentration of NB (mg/L); and C is the concentration of NB after photocatalytic reaction (mg/L).

2.6 Photodegradation kinetics

Langmuir–Hinshelwood kinetic models are often used to calculate photodegradation kinetic parameters, which are as follows [47]:

$$r = -\frac{dC}{dt} = -\frac{K_{ad}k'C}{1 + K_{ad}C}, \tag{3}$$

$$\frac{1}{r} = \frac{1}{K_{ad}k'C} + \frac{1}{k'}, \tag{4}$$

where r is the photodegradation reaction rate, k' is the rate constant of NB photocatalytic degradation, mg/(L min^{-1}); K_{ad} is the adsorption equilibrium constant of NB on catalyst surface, L/mg; C is the concentration of NB in solution, mg/L; and t is the reaction time, min.

The process of photocatalytic degradation begins with the catalyst surface adsorbing organic mass. C_e is the initial moment (t = 0) concentration of the solution while in adsorption equilibrium. The reaction time is calculated by the following equation:

$$t = \frac{1}{K_{ad}k'}\ln\left(\frac{C_e}{C}\right) + \frac{1}{k'}(C_e - C). \tag{5}$$

Formulae (3) and (5) can be simplified to formulae (6) and (7), respectively, when the organic content is extremely low. Formula (6) is also used for inefficient adsorption of organic mass. In this case, the reactions are manifested as first-order reactions.

$$r = -\frac{dC}{dt} = K_{ad}k'C = kC, \tag{6}$$

$$\ln\left(\frac{C_e}{C}\right) = K_{ad}k't = kt, \tag{7}$$

where k is the apparent rate constant, min^{-1}.

3 Results and discussion

3.1 Microtopography of SiO_2(AG)/T-ZnO

The microtopography of SiO_2(AG) and SiO_2(AG)/T-ZnO is demonstrated in Figure 1. As displayed in Figure 1a and c, SiO_2(AG) powders were composed of numerous narrow-size-range nanoparticles and presented loose sponge-like porous shapes. The SEM image of SiO_2(AG)/T-ZnO nanocomposites (Figure 1b) shows typical structures with four needles extending from the same center, ascribable to the T-ZnO [18] and SiO_2(AG) particles uniformly loaded on the surface of these needles. Figure 1(d) shows that the morphology of SiO_2(AG) loaded on the surface of T-ZnO has no obvious change.

3.2 Crystal structure of SiO_2(AG)/T-ZnO

As shown in Figure 2, a bread-like dispersion peak was observed in 2θ = 20–25°, which is the characteristic peak of amorphous SiO_2(AG) [48]. Other peaks corresponded with the characteristic peaks of the wurtzite ZnO structure [18]. The peaks of SiO_2(AG)/T-ZnO further indicated that SiO_2(AG) and T-ZnO still retained their crystal structural characteristics after forming SiO_2(AG)/T-ZnO composites.

3.3 SSA and pore structure of SiO_2(AG), T-ZnO, and SiO_2(AG)/T-ZnO

SSA and pore structure of SiO_2(AG), T-ZnO, and SiO_2(AG)/T-ZnO were analyzed via the N_2 adsorption–desorption method. As can be seen in Figure 3, N_2 adsorption–desorption isotherms of SiO_2 (AG), T-ZnO, and SiO_2(AG)/T-ZnO were type IV, II, and IV adsorption isotherms, respectively. Figure 3(a) indicates that SiO_2(AG) powders were porous materials, and the hole was a narrow tubular pore with open ends and wide mouth [49]. Figure 3(b) shows N_2 adsorption behavior on T-ZnO is gas physical absorption, which indicated that T-ZnO was a nonporous material [47]. Figure 3(c) shows that the SiO_2(AG) loaded on the surface of T-ZnO still maintained its original shape, and the adsorption of SiO_2(AG)/T-ZnO was significantly increased compared with T-ZnO. The SSA, pore size, and pore volume of SiO_2(AG), T-ZnO, and SiO_2(AG)/T-ZnO are shown in Table 1. Compared to T-ZnO, the SSA, pore size

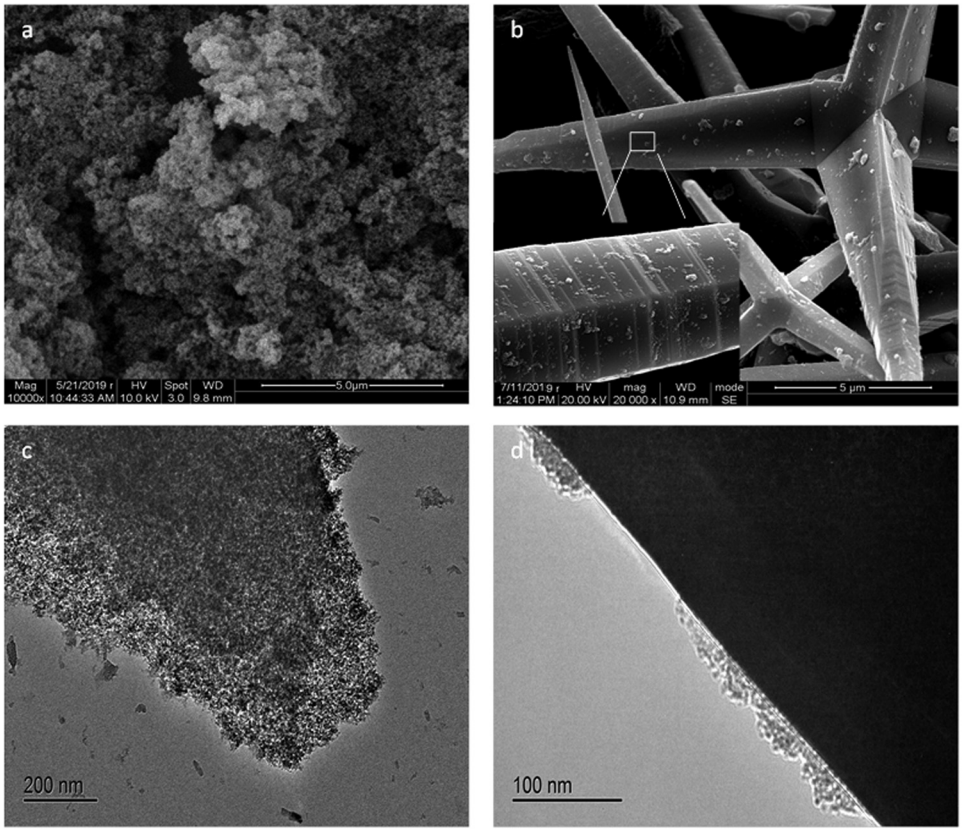

Figure 1: Morphologies of SiO_2(AG) and SiO_2(AG)/T-ZnO samples. (a) SEM image of SiO_2(AG); (b) SEM image of SiO_2(AG)/T-ZnO; (c) TEM image of SiO_2(AG); and (d) TEM image of SiO_2(AG)/T-ZnO.

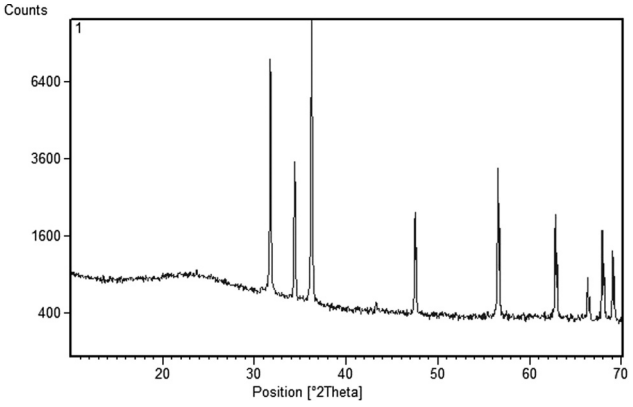

Figure 2: XRD pattern of SiO_2(AG)/T-ZnO sample.

distribution, and pore volume of SiO_2(AG)/T-ZnO were significantly improved.

3.4 UV-VIS DRS analysis

SiO_2(AG), T-ZnO, and SiO_2(AG)/T-ZnO were characterized by UV-VIS DRS. As shown in Figure 4, SiO_2(AG) had lower absorbance within the wavelength range between 200 and 800 nm. T-ZnO and SiO_2(AG)/T-ZnO showed strong absorption between 200 and 400 nm. Within the limits of visible light, the absorption of SiO_2(AG)/T-ZnO was enhanced slightly. The UV-VIS DRS of SiO_2(AG)/T-ZnO was similar to that of T-ZnO.

3.5 Adsorption property of T-ZnO and SiO_2(AG)/T-ZnO

Adsorption isotherms of T-ZnO and SiO_2(AG)/T-ZnO for NB are demonstrated in Figure 5. In the range of the organic concentration of this experiment, the adsorption amount of SiO_2(AG)/T-ZnO and T-ZnO to NB grew with the increase of the equilibrium concentration and equilibrium adsorption capacity up to 3.23 and 2.21 mg/g, respectively. T-ZnO had poor adsorption properties for NB because of small SSA of T-ZnO. The adsorption performance of SiO_2(AG)/T-ZnO was better than T-ZnO, because the SiO_2(AG) loaded on the surface of T-ZnO has good adsorption for NB [39].

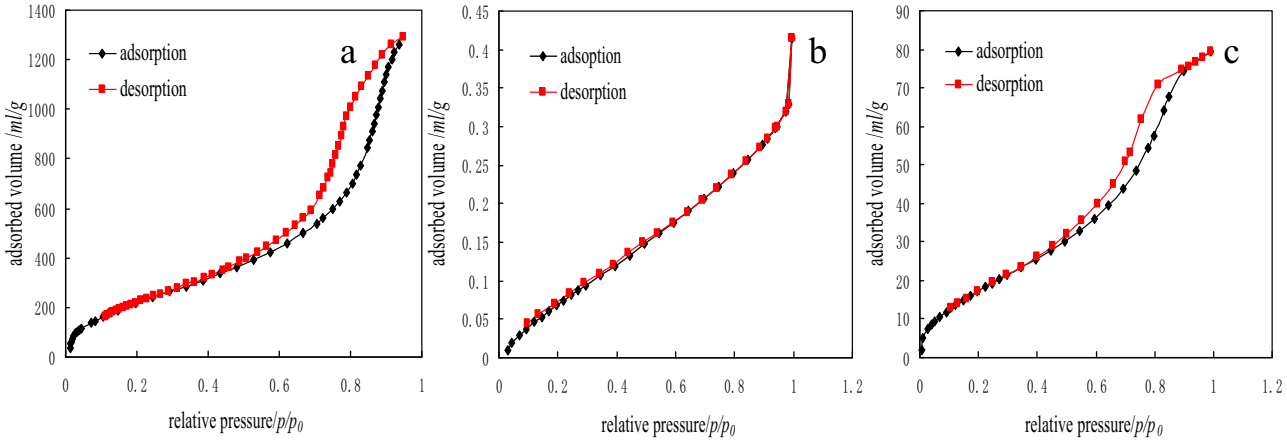

Figure 3: N_2 adsorption–desorption isotherm ((a) SiO_2(AG), (b) T-ZnO, and (c) SiO_2(AG)/T-ZnO).

3.6 Kinetic study of NB degradation by T-ZnO and SiO_2(AG)/T-ZnO

The NB photocatalytic degradation curves of T-ZnO and SiO_2(AG)/T-ZnO are shown in Figure 6. Compared to T-ZnO, SiO_2(AG)/T-ZnO had better photocatalytic effect for NB with different initial concentrations. The degradation processes of different initial concentrations of NB were fitted by the pseudo first-order kinetic equation. Figure 7 obviously indicates that the degradation processes of NB by T-ZnO and SiO_2(AG)/T-ZnO followed the first-order reaction.

Considering the initial moment reaction kinetic, the curves of $1/C_e$ and $1/r_0$ are displayed in Figure 8, and the relevant fitting equations are as follows:

$$\text{SiO}_2\text{(AG)/T-ZnO: } \frac{1}{r_0} = \frac{35.397}{C_0} + 4.1307 \quad R^2 = 0.976,$$

$$\text{T-ZnO: } \frac{1}{r_0} = \frac{63.695}{C_0} + 6.7816 \quad R^2 = 0.9915.$$

The degradation kinetics of SiO_2(AG)/T-ZnO and T-ZnO were consistent with the Langmuir–Hinshelwood

Table 1: SSA, pore size, and pore volume of SiO_2(AG), T-ZnO, and SiO_2(AG)/T-ZnO

Sample	SiO_2(AG)	T-ZnO	SiO_2(AG)/T-ZnO
SSA (m^2/g)	896	0.4310	86.8132
Pore size (nm)	8.93	—	7.08
Pore volume (mL/g)	2.0065	0.0006	0.1418

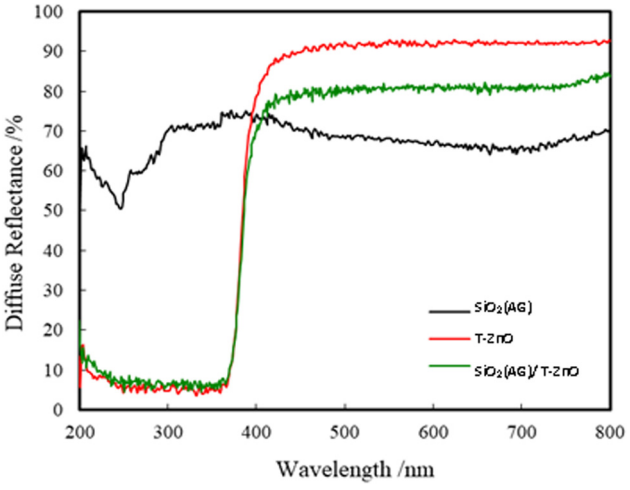

Figure 4: UV-Visible diffuse reflectance spectra of SiO_2(AG), T-ZnO, and SiO_2(AG)/T-ZnO.

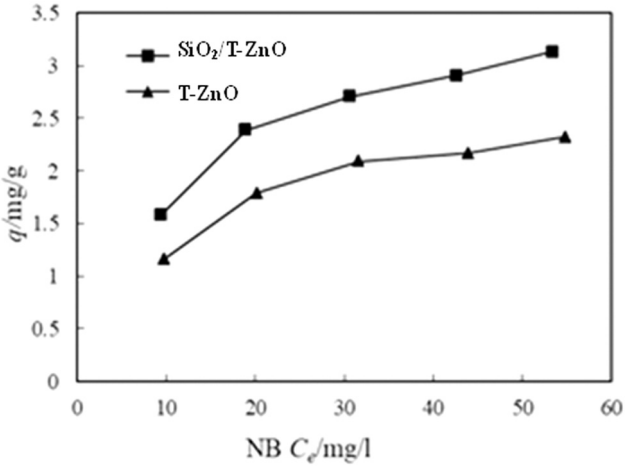

Figure 5: Adsorption isotherms of NB by T-ZnO and SiO_2(AG)/T-ZnO.

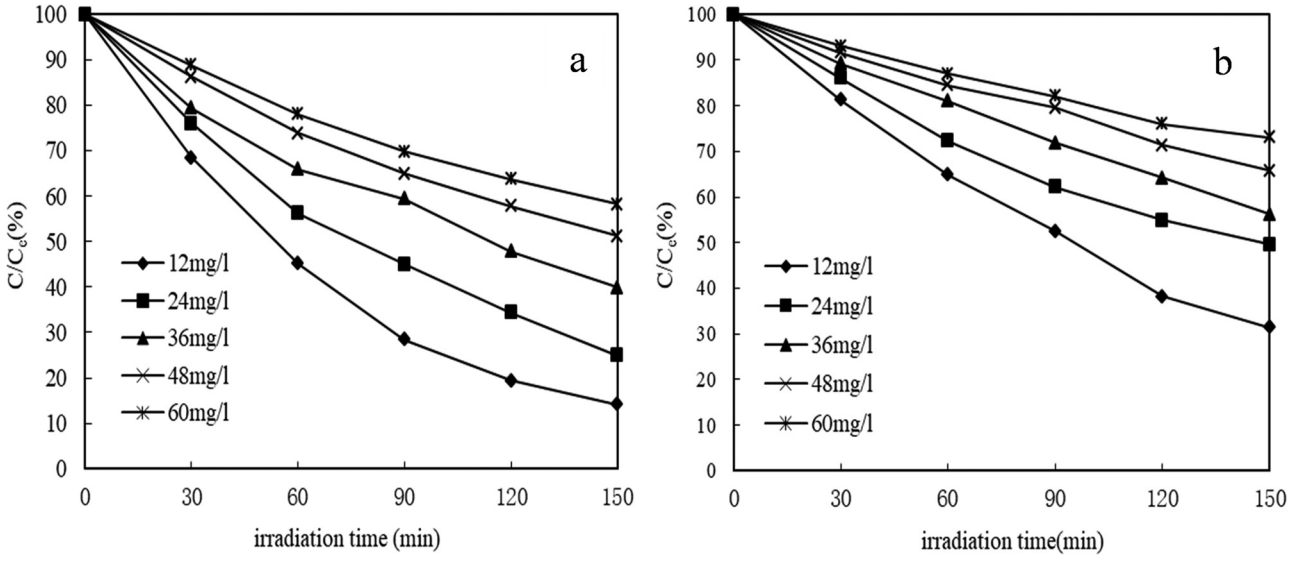

Figure 6: Degradation curves of different initial concentrations of NB by SiO_2(AG)/T-ZnO (a) and T-ZnO (b).

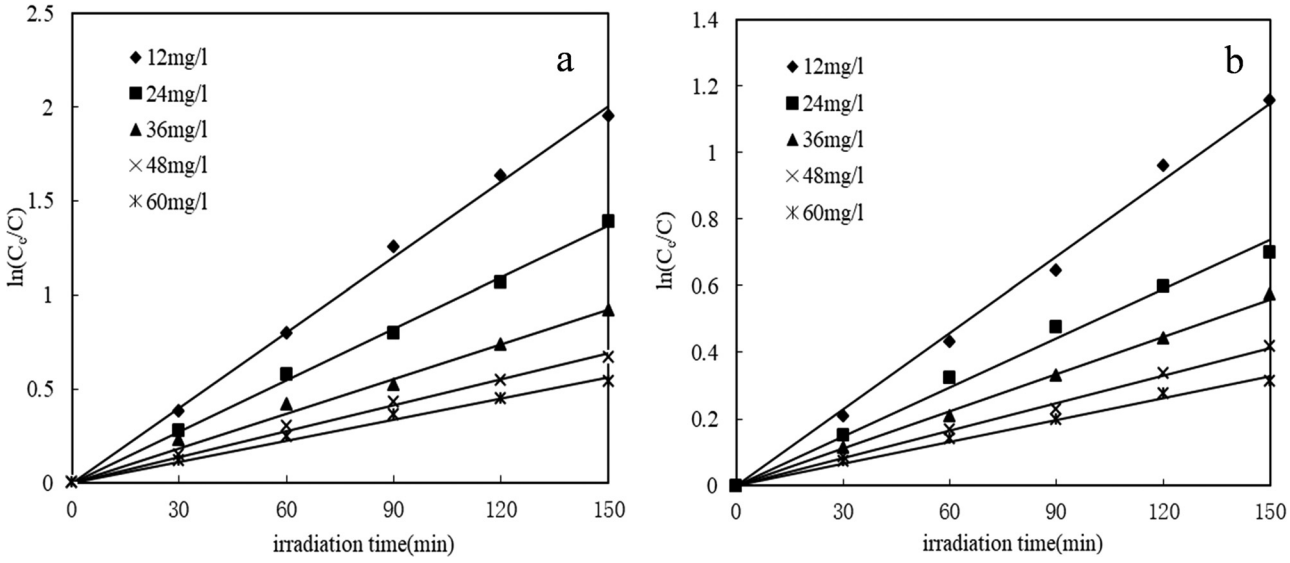

Figure 7: Degradation-fitting curves of NB by SiO_2(AG)/T-ZnO (a) and T-ZnO (b).

kinetic model. The degradation rate constant and adsorption constant of NB using SiO_2(AG)/T-ZnO and T-ZnO could be calculated, which were k' = 0.2421 mg/L min^{-1}, K_{ad} = 0.1167 L/mg and k' = 0.1475 mg/L min^{-1}, K_{ad} = 0.1065 L/mg. The results indicated that $k'_{SiO_2(AG)/T\text{-}ZnO} > k'_{T\text{-}ZnO}$, $K_{ad\ SiO_2(AG)/T\text{-}ZnO} > K_{ad\ T\text{-}ZnO}$. According to the phenomenon, we concluded that the loading of SiO_2(AG) could increase T-ZnO adsorption to NB, and then promoted photocatalysis.

4 Conclusion

SiO_2(AG)/T-ZnO composites were prepared via a simple and controllable method. Various characterization methods showed that the morphology and structural characteristics of SiO_2(AG) and T-ZnO were retained after SiO_2(AG) loading on the surface of T-ZnO. The photocatalytic degradation processes of NB using T-ZnO and SiO_2(AG)/T-ZnO followed the first-order reaction. SiO_2

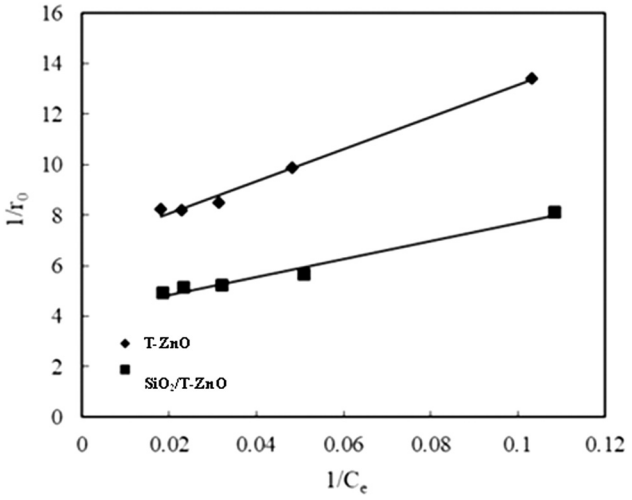

Figure 8: Curves of $1/C_e$ and $1/r_0$ of NB degradation.

(AG)/T-ZnO had better photocatalytic performance. Considering the initial moment reaction kinetic, the photocatalytic kinetic of SiO_2(AG)/T-ZnO and T-ZnO was consistent with the Langmuir–Hinshelwood kinetic model, and reaction rate constant $k'_{SiO_2(AG)/T\text{-}ZnO} > k'_{T\text{-}ZnO}$, adsorption rate constant $K_{ad\ SiO_2(AG)/T\text{-}ZnO} > K_{adT\text{-}ZnO}$, which demonstrated SiO_2(AG) loading could increase T-ZnO adsorption to NB, then promoted its photocatalytic performance. Compared with the conclusions of the important relevant papers of this study, loading SiO_2(AG) on the surface of T-ZnO can retain the morphology and structural characteristics of T-ZnO and SiO_2(AG) unchanged, and the photocatalysis of SiO_2(AG)/T-ZnO composites for NB can be significantly improved. The improvement of the catalytic performance of the material by this method is better than that of other porous materials combined with semiconductor materials.

Acknowledgments: This work was supported by the National Natural Science Foundation of China (No. 21507052), Project of Introduction of Teachers of Leshan Normal University, Sichuan Province, China (Grant No. Z1517), and Scientific Research Fund of Leshan Normal University, Sichuan Province, China (Grant No. 205190012).

Author contributions: Zhigang Yi designed the experiments, contributed to characterization of materials, and led the drafting of the manuscript. Tao Jiang and Ying Cheng assisted in the analysis and testing work during the experiments. Qiong Tang designed and supervised the experiments.

Conflict of interest: The authors declare no conflict of interest regarding the publication of this paper.

Data accessibility: The authors conducted the experiment systematically and reported experimental procedure clearly in Section 2 and provided all necessary data in Section 3 of the manuscript.

References

[1] Wu T, Ding X, Su B, Soodeen-Lalloo A.K, Zhang L, Shi JY Magnetic resonance imaging of tumor angiogenesis using dual-targeting RGD10-NGR9 ultrasmall superparamagnetic iron oxide nanoparticles. Clin Transl Oncol. 2018;20:599–606.
[2] Jia F, Li G, Yang B, Yu B, Shen Y, Cong H Investigation of rare earth upconversion fluorescent nanoparticles in biomedical field. Nanotechnol Rev. 2019;8:1–17.
[3] Bakand S, Hayes A, Dechsakulthorn F. Nanoparticles: a review of particle toxicology following inhalation exposure. Inhal Toxi-col. 2012;24:125–35.
[4] Pantic S, Radojevic Skodric S, Loncar Z, Pantic I. Neurotoxicity, nephrotoxicity, and hepatotoxicity of copper-based nanoparticles: potential implications in molecular medicine and neurosciences. Rev Adv Mater Sci. 2019;10:201–5.
[5] Liu Y, Jia M, Song C, Lu S, Wang H, Zhang G, Yang Y. Enhancing ultra-early strength of sulphoaluminate cement-based materials by incorporating grapheme oxide. Nanotechnol Rev. 2020;9:17–27.
[6] Zhang C, Hu M, Dong L, Gebremariam A, Miranda-Xicotencatl B, Di Maio F, Tukker A. Eco-efficiency assessment of technological innovations in high-grade concrete recycling. Resour Conserv Recycl. 2019;149:649–63.
[7] Zhang H, Zhao Y, Meng T, Shah SP. The modification effects of a nanosilica slurry on microstructure, strength, and strain development of recycled aggregate concrete applied in an enlarged structural test. Constr Build Mater. 2015;95:721–35.
[8] Parihar V, Raja M, Paulose R. A brief review of structural, electrical and electrochemical properties of zinc oxide nanoparticles. Rev Adv Mater Sci. 2019;3:119–30.
[9] Wei J, Wei S, Zia Ur R, Wang DA. Recent progress in red semiconductor photocatalysts for solar energy conversion and utilization. Nanotechnol Rev. 2016;5:135–45.
[10] Fukahori S, Fujiwara T. Photocatalytic decomposition behavior and reaction pathway of sulfamethazine antibiotic using TiO_2. J Env Manag. 2015;157:103–10.
[11] Yang Q, Chen G, Zhang J, Li H. Adsorption of sulfamethazine by multi-walled carbon nanotubes: effects of aqueous solution chemistry. RSC Adv. 2015;5:25541–9.
[12] Elena CP, Sara GS. Controlled synthesis and microstructural-properties of Sol-Gel TiO2 nanoparticles for photocatalytic cement composites. Nanomaterials. 2019;9:1–16.
[13] Li J, Liu H, Deng Y, Liu G, Chen Y, Yang J. Emerging nanostructured materials for the catalytic removal of volatile organic compounds. Nanotechnol Rev. 2016;5:147–81.
[14] Bozkurt Çırak B, Caglar B, Kılınç T, Morkoç Karadeniz S, Erdoğan Y, Kılıç S, Kahveci E, Ercan Ekinci A, Çırak Ç. Synthesis

and characterization of ZnO nanorice decorated TiO2 nanotubes for enhanced photocatalytic activity. Mater Res Bull. 2019;109:160–7.
[15] Keane D, Basha S, Nolan K, Morrissey A, Oelgemller M, Tobin JM. Photodegradation of famotidine by integrated photocatalytic adsorbent (IPCA) and kinetic study. Cata Lett. 2011;141:300–08.
[16] Kanakaraju D, Ravichandar S, Lim YC. Combined effects of adsorption and photocatalysis by hybrid TiO_2/ZnO-calcium alginate beads for the removal of copper. J Env Sci. 2017;55:214–23.
[17] Xu Y, Yin JC, Wang J, Wang XB. Design and optimization of solar steam generation system for water purification and energy utilization: a review. Rev Adv Mater Sci. 2019;11:226–47.
[18] Yi Z, Wang J, Jiang T, Tang Q, Cheng Y. Photocatalytic degradation of sulfamethazine in aqueous solution using ZnO with different morphologies. R Soc Open Sci. 2018;5:171457–68.
[19] Yi Z, Wang J, Tang Q, Jiang T. Photolysis of sulfamethazine using UV irradiation in an aqueous medium. RSC Adv. 2018;8:1427–35.
[20] Gupta VK, Kumar R, Nayak A, Saleh TA, Barakat MA. Adsorptive removal of dyes from aqueous solution onto carbon nanotubes: a review. Adv Colloid Interfac. 2013;193–4:24–34.
[21] Lin Y, Xu J, Sudhakar BS, Gu J, Hong R. Preparation of spherical aminopropyl-functionalized MCM-41 and its application in removal of Pb(II) ion from aqueous solution. Nanotechnol Rev. 2019;8:275–84.
[22] Wang J, Lu H, Zhou Y, Song Y, Liu G, Feng Y. Enhanced biotransformation of nitrobenzene by the synergies of Shewanella species and mediator-functionalized polyurethane foam. J Hazard Mater. 2013;252–3:227–32.
[23] Jeong S, Lee H, Park H, Jeon KJ, Park YK, Jung SC. Rapid photocatalytic degradation of nitrobenzene under the simultaneous illumination of UV and microwave radiation fields with a TiO_2 ball catalyst. Catal Today. 2018;307:65–72.
[24] Sun Z, He X, Du J, Gong W. Synergistic effect of photocatalysis and adsorption of nano-TiO_2 self-assembled onto sulfanyl/activated carbon composite. Env Sci Pollut R. 2016;23:21733–40.
[25] Reszczyńska J, Grzyb T, Sobczak JW, Lisowski W, Gazda M, Ohtani B, Zaleska A. Visible light activity of rare earth metal doped (Er^{3+}, Yb^{3+} or Er^{3+}/Yb^{3+}) titania photocatalysts. Appl Catal B-Environ. 2015;163:40–49.
[26] Pandiyarajan T. Sonochemical synthesis of CuO nanostructures and their morphology dependent optical and visible light driven photocatalytic properties. J Mater Sci Mater Electron. 2017;28:2448–57.
[27] Xie J, Li Y, Zhao W, Bian L, Wei Y. Simple fabrication and photocatalytic activity of ZnO particles with different morphologies. Powder Technol. 2011;207:140–4.
[28] Logothetidis S, Laskarakis A, Kassavetis S, Lousinian S, Gravalidis C, Kiriakidis G. Optical and structural properties of ZnO for transparent electronics. Thin Solid Films. 2008;516:1345–9.
[29] Pantic S, Skodric SR, Loncar Z, Pantic I. Zinc oxide nanoparticles: potential novel applications in cellular physiology, pathology, neurosciences and cancer research. Rev Adv Mater Sci. 2019;4:17–21.
[30] Hariharan C. Photocatalytic degradation of organic contaminants in water by ZnO nanoparticles: revisited. Appl Catal, A. 2006;304:55–61.
[31] Khodja AA, Sehili T, Pilichowski JF, Boule P. Photocatalytic degradation of 2-phenylphenol on TiO_2 and ZnO in aqueous suspensions. J Photochem Photobiol, A. 2001;141:231–9.
[32] Kansal SK, Singh M, Sud D. Studies on photodegradation of two commercial dyes in aqueous phase using different photocatalysts. J Hazard Mater. 2007;141:581–90.
[33] Sobana N, Swaminathan M. The effect of operational parameters on the photocatalytic degradation of acid red 18 by ZnO. Sep Purif Technol. 2007;56:101–7.
[34] Maasumeh K, Zahra A. Efficient adsorption-photodegradation of 4-nitrophenol in aqueous solution by using ZnO/HZSM-5 nanocomposites. Desalination. 2012;286:428–253.
[35] Typek J, Guskos N, Zolnierkiewicz G, Pilarska M, Guskos A, Kusiak-Nejman E, Morawski AW. Magnetic properties of TiO_2/graphitic carbon nanocomposites. Rev Adv Mater Sci. 2019;6:107–22.
[36] Yang SJ, Im JH, Kim T, Lee K, Park CR. MOF-derived ZnO and ZnO@C composites with high photocatalytic activity and adsorption capacity. J Hazar Mater. 2011;186:376–82.
[37] Yoneyama H, Torimoto T. Titanium dioxide/adsorbent hybrid photocatalysts for photodestruction of organic substances of dilute concentrations. Catal Today. 2000;58:133–40.
[38] Liu F, Leung YH, Djurišić AB, Ng AMC, Chan WK. Native defects in ZnO: effect on dye adsorption and photocatalytic degradation. J Phys Chem C. 2013;117:12218–28.
[39] Yi ZG, Tang Q, Jiang T, Cheng Y. Adsorption performance of hydrophobic/hydrophilic silica aerogel for low concentration organic pollutant in aqueous solution. Nanotechnol Rev. 2019;8:266–74.
[40] Tryba B, Tsumura T, Janus M, Morawski AW, Inagaki M. Carbon-coated anatase: adsorption and decomposition of phenol in water. Appl Catal B-Environ. 2004;50:177–83.
[41] Shi J, Chen J, Feng Z, Chen T, Wang X, Ying P, Li C. Time-resolved photoluminescence characteristics of subnanometer ZnO clusters confined in the micropores of zeolite. J Phys Chem B. 2006;110:25612–8.
[42] Chen J, Feng ZhCh, Ying PL, Li C. ZnO clusters encapsulated inside micropores of zeolites studied by UV raman and laser-induced luminescence spectroscopies. J Phys Chem B. 2004;108:12669–76.
[43] Hrubesh LW, Coronado PR, Satcher JH. Solvent removal from water with hydrophobic aerogels. J Non-Cryst Solid. 2001;285:328–32.
[44] Reynolds JG, Coronado PR, Hrubesh LW. Hydrophobic aerogels for oil-spill clean up synthesis and characterization. J Non-Cryst Solid. 2001;292:127–37.
[45] Zhou ZW, Deng H. A new method for preparation of ZnO oxide whiskers. Mater Res Bull. 1999;34:1563–7.
[46] Prakash SS, Brinker CJ, Hurd AJ, Rao SM. Silica aerogel films prepared at ambient pressure by using surface derivatization to induce reversible drying shrinkage. Nature. 1995;374:439–43.
[47] Hasnat MA, Uddin MM, Samed AJF. Adsorption and photocatalytic decolorization of a synthetic dye erythrosine on anatase TiO_2 and ZnO surfaces. J Hazar Mater. 2007;147:471–7.
[48] Zhu JJ, Yao J, Lu XM, Ding JL, Du FH, Xie JM. Synthesis and characterization of super hydrophobic mesoporous silica aerogels by ambient pressure drying. J Chin Ceram Soc. (in chinese), 2009;37:512–5.
[49] Yan JM, Zhang JY. Adsorption and condensation-surface and pore in solid. Beijing: Science Press; 1979.